A Comparison of Robust Coherence Factor Implementations

Carl-Inge C. Nilsen, *Member, IEEE,* Andreas Austeng, *Member, IEEE*

***Abstract*—The Coherence Factor (CF) was introduced as a metric to quantify the amount of phase aberrations in an ultrasound image, and has also been incorporated into the actual beamforming algorithm. Its function has been described as both reducing the effects of phase aberrations and as general noise reduction. It is well known that, when the CF is included in the beamformer, the resulting images suffer from certain artifacts when the signal-to-interference-and-noise ratio is low. Two different robustness measures have been introduced to mitigate these artifacts: the Generalized Coherence Factor (GCF) and the Scaled Wiener Postfilter (SWiP). However, a comparison of these robust methods has not yet been performed. In this paper we compare GCF and SWiP, and verify their respective tradeoffs between performance and robustness through simulations that include scenarios with and without phase aberrations. We find that when robustness is identically increased in the two methods, SWiP will generally retain the best performance with respect to cyst contrast ratio and point resolution.**

***Index Terms*—Ultrasound imaging, adaptive beamforming, coherence factor, Wiener postfilter, robustness, phase aberrations**

I. Introduction

Adaptive, data-dependent beamforming methods are used in ultrasound imaging to augment conventional, static beamformers and increase image quality. Several methods have been applied to ultrasound imaging, one of which is the Coherence Factor (CF) [1], also known as the Mallart-Fink focusing factor [2], [3]. The CF is used to estimate the local quality or reliability throughout the entire image, and use these estimates to attenuate the low-quality regions while preserving the ones with higher quality. The quality estimator is based on the ratio of coherent to total energy across the array for a single pixel in the output image. The assumption behind such an estimator is that coherent energy is the result of an actual, desired echo while incoherent energy is due to noise, interference, or phase aberrations. CF-based methods are now used for general image improvement, even though they were originally suggested to measure and reduce the effects of phase aberrations specifically [1], [4]. The effectiveness of CF-based methods has been demonstrated for applications such as breast cancer detection [5] and non-destructive evaluation (NDE) of materials [6]. The methods have also been applied to other imaging modalities such as UWB radar [7], [8]. The CF can be combined with other adaptive beamformers [9], [10], [11], such as the Minimum Variance beamformer [12], which has been shown to result in an implementation of the Wiener beamformer [13]. Other variations on CF exist, such as a phase-based coherence factor shown to attenuate grating lobes [14] and a short-lag spatial coherence method that is used for clutter reduction [15].

Robustness is an important issue for all adaptive algorithms, and it is well known that the original CF is prone to artifacts when the Signal-to-Interference-and-Noise Ratio (SINR) is low. These artifacts manifest themselves as regions with severely underestimated magnitudes in the image, e.g. as "black holes" in speckle regions near strong scatterers. Li and Li considered such artifacts in [4], and suggested the Generalized Coherence Factor (GCF) as a possible solution. The GCF achieves robustness by gradually widening the definition of what is considered as coherent energy. Another robust implementation, the Scaled Wiener Postfilter (SWiP), was later suggested in [13]. SWiP is derived from an interpretation of the CF as an Minimum Mean Square Error (MMSE) estimator that overestimates the amount of noise in the data. Both the GCF and SWiP methods sacrifice some performance to achieve increased robustness against artifacts in low-SINR scenarios.

In this paper we describe the differences between the GCF and SWiP methods and the reasons for their increased robustness. Because the two methods are derived in quite different ways and achieve increased robustness by different means, they are not easily compared with respect to performance. We suggest one possible basis for comparison, namely the relationship between image enhancement and robustness against artifacts, which is used to rank the methods through simulations. The simulations cover scenarios with speckle targets and point scatterers, for situations with or without the effects of phase aberrations.

In Sec. II we present the necessary background theory on beamforming, as well as the CF, GCF, and SWiP methods. In Sec. III we suggest a metric for comparing the GCF and SWiP as robust implementations of the CF, and investigate it using simulations. In Sec. IV we present our conclusions.

II. Background

Our application is a phased array imaging system, which creates an ultrasound image by insonifying a medium with a focused pulse and subsequently forming a scan line from the received echoes. This process is repeated for adjacent scan lines, resulting in a sector image. The imaging application

The authors are with the Center for Imaging/Department of Informatics at the University of Oslo. This work has been partially financed by the Norwegian Research Council project "Acoustic Imaging and Interpretation"

Manuscript received XX XX, 2012.

could be either medical imaging or NDE. We will assume an M-element uniform linear array (ULA), recording a data vector $\vec{x}[n] \in \mathbb{C}^M$. The data vector contains a narrowband signal of interest, interfering narrowband sources, and spatially white noise:

$$\vec{x}[n] = A[n]\vec{d} + \vec{p}[n], \tag{1}$$

where n represents the range or time index. The amplitude of interest is given by $A[n]$ and the signal propagation vector is given by $\vec{d}$. We assume that steering and focusing has been applied to the data, so we have $\vec{d} = \vec{1}$. The unwanted noise and interference is contained in $\vec{p}[n]$. Our goal is to obtain an estimate of the signal amplitude $A[n]$ from the data vector $\vec{x}[n]$ by properly attenuating the contribution from the noise and interference in $\vec{p}[n]$. A common technique is delay-and-sum (DAS) beamforming. The DAS beamformer creates a weighted sum of the data vector elements, yielding an output:

$$y_{DAS}[n] = \vec{w}_{DAS}^H \vec{x}[n], \tag{2}$$

where $\vec{w}$ is the weight vector.

A. The Coherence Factor

There are several beamforming methods that offer improvements over the conventional method described by (2), e.g. adaptive beamformers. One possibility when designing an adaptive beamformer is to utilize a varying and situation-dependent weight vector $\vec{w}[n]$ that is optimal with respect to some criterion, such as the Minimum Variance beamformer [12], [16], [17]. Another possibility is to use a static weighting function as in (2), but subsequently scale the output using an adaptive scalar postfilter. Compared to e.g. MV beamforming, these methods have significantly reduced computational complexity. The postfiltered DAS output can be written as:

$$y_{PF}[n] = H[n]y_{DAS}[n] = H[n]\vec{w}_{DAS}^H \vec{x}[n], \tag{3}$$

where the postfilter, $H[n]$, takes a value in the range $[0, 1]$ to compensate for any remaining noise or interference in $y_{DAS}[n]$. For simplicity, the dependence on the sample index n will be suppressed for the remainder of the article. The Coherence Factor is an example of such a postfilter:

$$H_{CF} = \frac{\left|\sum_{m=0}^{M-1} x_m\right|^2}{M\sum_{m=0}^{M-1}|x_m|^2}. \tag{4}$$

In [4], Li and Li show that the inclusion of H_{CF} in the beamformer decreased the effects of phase aberrations. It was also demonstrated that when SINR is low, images weighted by the CF contain certain artifacts. An example of this is shown in Fig. 1 **a)** and **b)**. In the former, we see a massive cyst in speckle, imaged using a uniformly weighted DAS beamformer. Its edges are blurry, due to sidelobe leakage from the cyst into the speckle. In the latter, we see the CF-postfiltered image. Here, the cyst edges are more clearly defined than in the DAS image. However, the speckle surrounding the cyst is significantly attenuated in the lateral direction, creating the impression of empty regions. These are examples of the low-SINR artifacts of CF, which motivated the development of robust postfilter alternatives that could retain some of CF's desired properties while not experiencing the same amount of distortion.

B. Generalized Coherence Factor

The Generalized Coherence Factor was suggested by Li and Li in [4] as a robust alternative to the CF. The GCF works by first converting the element data vector $\vec{x}$ to an orthogonal beamspace vector $\vec{X} = \left[X_{-(M-1)/2+1}, \cdots, X_0, \cdots, X_{(M-1)/2}\right]^T$. For a uniform linear array, this is done using a spatial Discrete Fourier Transformation (DFT) or, in practice, a Fast Fourier Transformation (FFT). Each DFT coefficient represent a beam steered to a different off-broadside angle. The set of DFT coefficients is usually referred to as a beamspace, which can be utilized in different ways in adaptive beamformers. More details about beamspace transformations for ultrasound imaging can be found in e.g. [18], where they are used to reduce the computational complexity in the MV beamformer. The sum in the denominator of the CF expression in (4) can be written in terms of the beamspace instead of the element signals through Parseval's identity. The numerator of (4) corresponds to X_0, i.e. the DFT coefficient of index 0. GCF achieves robustness by adding $2K_0$ of the adjacent DFT coefficients to the numerator, starting with indices ± 1, ± 2, etc. The GCF that averages over $2K_0 + 1$ such beams is given as:

$$H_{GCF}(K_0) = \frac{\sum_{k=-K_0}^{K_0}|X_k|^2}{\sum_{k=-(M-1)/2+1}^{(M-1)/2}|X_k|^2}. \tag{5}$$

For $K_0 = 0$ we get $H_{GCF}(0) = H_{CF}$, i.e. the GCF becomes the CF as defined in (4). For $K_0 = M/2$ we get $H_{GCF}(M/2) = 1$, i.e. the GCF has no effect and the postfiltered output (3) does not differ from the ordinary DAS output (2). The GCF was shown to give increased robustness against low SINR, while retaining some of the performance of the CF [4]. This is demonstrated in Fig. 1 **c)**, where we see that the black holes in the speckle are gradually filled in. Unfortunately, the sharp edge of the cyst is also degraded.

C. Scaled Wiener Postfilter

The Scaled Wiener Postfilter was suggested as a postfilter for ultrasound imaging in [13]. It is a robust generalization of the Wiener postfilter, which minimizes the Mean Square Error of the beamformer output. The SWiP corresponding to a uniformly weighted DAS beamformer is given as:

$$H_{SWiP}(\alpha) = \frac{|\bar{x}|^2}{|\bar{x}|^2 + \frac{\alpha}{M^2}\sum_{m=0}^{M-1}|x_m - \bar{x}|^2}$$
$$\text{where } \bar{x} = \frac{1}{M}\sum_{m=0}^{M-1} x_m = y_{DAS} \text{ for } \vec{w}_{DAS} = \frac{1}{M}\vec{1}. \tag{6}$$

For $\alpha = M$ we get $H_{SWiP}(M) = H_{CF}$, i.e. SWiP becomes the CF in (4). For $\alpha = 1$ SWiP becomes the true Wiener postfilter [13]. If $\alpha = 0$ we get $H_{SWiP}(0) = 1$, i.e. SWiP has no effect and the postfiltered output is identical to the conventional DAS output. The increased robustness of the SWiP compared to the CF has been demonstrated in [13]. Note that the SWiP-implementation of (6) implicitly assumes that the noise component is spatially white. There is an alternative

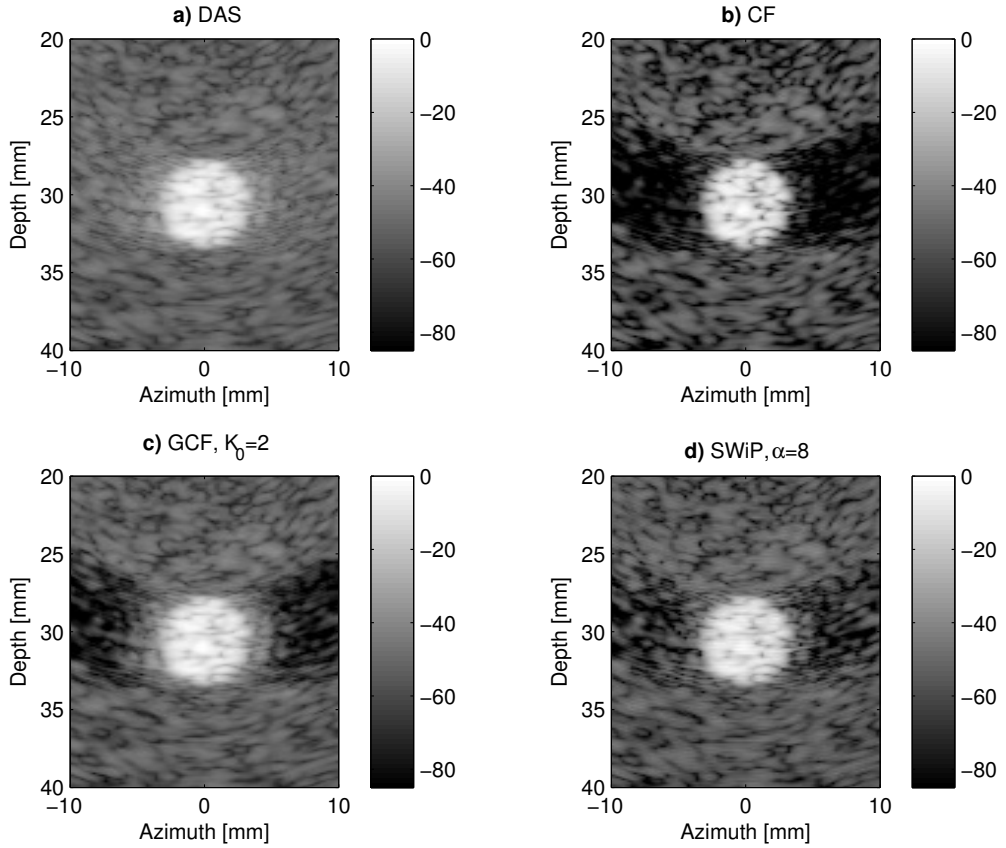

Fig. 1. Low-SINR artifacts in uniform speckle area around a massive cyst. 64 element ULA. **a)** DAS **b)** CF **c)** GCF w/$K_0 = 2$ **d)** SWiP w/$\alpha = 8$. Images displayed with 85 dB dynamic range.

implementation of SWiP that does not make assumptions about the spatial characteristics of noise [13]. However, as this solution does not reduce to the CF, we will not investigate it further it in this paper. The effect of SWiP is illustrated in Fig. 1 **d)**. We see a similar effect as GCF, in that speckle in the empty regions surrounding the massive cyst is gradually restored.

D. Relationships Between CF, GCF, and SWiP

If we examine the SWiP expansion of the CF (i.e. (6) with $\alpha = M$), we can isolate the reason for the low-SINR artifacts. A large amount of interference or noise in the data will significantly increase the denominator of the CF, making the whole fraction decrease towards zero. The increased denominator would not pose a problem if the interference-and-noise level were relatively constant throughout the entire image. In this case, the result would be a constant decrease of the CF, yielding an output image with a constant decrease in magnitude. However, when the interference-and-noise level is spatially variant, the CF will fluctuate throughout the image. Areas of increased noise will for instance appear around strong point scatterers or massive objects creating the before mentioned "black hole"-artifact regions that were shown in Fig. 1.

If we want the CF to be more robust against these fluctuating interference-and-noise levels, it is intuitively clear that we must do one of two things; either increase the numerator of (4) by some amount proportional to the interference and noise, or alternatively decrease the part of the denominator that represents the interference and noise. The GCF seeks to implement the first solution, while SWiP is an attempt to implement the second solution. Note that GCF and SWiP have the same end-points at opposite directions of the parameter scale; for GCF $K_0 = 0$ corresponds to the CF and $K_0 = K$ yields $H_{GCF} = 1$. For SWiP, $\alpha = M$ yields the CF and $\alpha = 0$ yields $H_{SWiP} = 1$.

One difference between the two methods is that the SWiP can be made even more aggressive than the CF, by increasing α beyond M. (Note that a similar result is achievable with GCF if it were further generalized, with some sort of weighting function introduced in the numerator sum.) Another difference is that SWiP has a continuous parameter that directly determines the robustness by adjusting the degree of noise overestimation, while GCF has a discrete parameter which only indirectly determines the robustness that ultimately depends on the actual distribution of noise in the spatial DFT coefficients. An indication of the different effects of GCF and SWiP can be seen by comparing Fig. 1 **c)** and Fig. 1 **d)**. Both methods

restore speckle around the massive cyst, however, GCF affects primarily the cyst's immediate surroundings while SWiP has a more spatially uniform effect. In addition, the cyst edges in the GCF image seem slightly more blurry than in the SWiP image. Unfortunately there is no way of expressing the general GCF expression of (5) using the SWiP expression of (6) or vice versa, and therefore a practical, performance-based comparison of the two methods is required.

III. Results and Discussion

A. Simulations and Performance

Ideally, we would like to perform a general, theoretical comparison between the performances of GCF and SWiP. However, their different behavior is situation dependent, so no satisfactory general comparison can be made. Therefore, we will need to compare the two methods with respect to specific performance metrics for some representative simulated scenarios. We have chosen to investigate the methods' abilities to enhance two metrics: the point scatterer resolution and the Contrast Ratio (CR). We investigate resolution and CR performance for situations with and without phase aberrations.

Our chosen definition of the resolution of the beamformer is the smallest angular separation that two point scatterers can have while being represented in the image as two distinct peaks with a 3 dB dip in between. While not an original application of the CF, the fact that such methods can reduce the minimum separation for 3dB resolution has been demonstrated in e.g. [14]. Note that the resolution metric is not necessarily sensitive to the low-SINR artifacts of CF methods. The reason for this is that resolution is determined by the relative difference between two point scatterer peaks and the dip in between, which may be equally large even if the absolute peak magnitudes themselves are falsely estimated due to the previously described artifacts.

The contrast ratio is defined as the ratio of the mean value in the background speckle to the mean value inside an anechoic cyst [19]. Neither this metric is necessarily sensitive to the low-SINR artifacts of the CF, because it only responds to the relative difference between regions and does not require the correct estimation of absolute speckle magnitudes.

Because both these metrics may be insensitive to low-SNR distortions, we need an additional metric to measure these undesired effects. We will attempt to quantify them by calculating the corresponding Root Mean Square Error (RMSE) of the echo from a single point scatterer in spatially white noise at a given SINR for all values of $K_0 = 0, 1, \cdots, M/2$ and $\alpha \in [0, M]$. The RMSE will typically increase with the low-SINR distortions of the CF-based methods. It is assumed that postfilter behavior for more complex scenarios, like the massive cyst in Fig. 1, can be extrapolated from this simple example.

It has previously been shown that while the CF may increase performance beyond that of ordinary DAS for certain metrics like CR and resolution, this ability is reduced for both the GCF [4] and SWiP [13] methods when their parameters are adjusted to provide more robustness against low-SINR distortions. However, it has not been established just how much performance that must be sacrificed to gain a certain amount of robustness. The question is, if the GCF and SWiP are adjusted to obtain some specific, identical degree of image quality improvement in between DAS and CF, which of them is superior in the sense of having the smallest estimation error for the point scatterer magnitude? Alternatively; if GCF and SWiP are adjusted to provide identical amounts of robustness, as measured by point scatterer RMSE, which of them yields the superior CR and resolution?

The comparison is done using Field II simulations [20], [21] of anechoic cysts and point scatterers. We simulate a 64 element uniform linear array with center frequency 3.5 MHz and half-wavelength spacing, imaging a cyst with radius 3 mm placed at 40 mm depth to investigate the contrast ratio, and point scatterers placed at depth 40 mm to investigate resolution and RMSE, as shown in Fig. 2. The upper row of Fig. 2 shows the scenarios without the effects of phase aberrations, while the lower row shows how phase aberrations decreases contrast (left hand side) and distorts point scatterers (right hand side). First we will investigate the case of no phase aberrations. Fig. 3 demonstrates the effects of adjusting the parameters (K_0 and α) on cyst contrast ratio and RMSE. We observe, in Fig. 3 **a)**, that the CR of GCF decreases rapidly for increasing K_0, while that of SWiP is only affected for very low values of α. We make the same observation for resolution, as shown in Fig. 3 **c)**, where it is seen that increasing the parameter of GCF results in a rapidly decreasing resolution, which almost instantly converges to that of DAS. SWiP, on the other hand, experiences a much slower decrease of resolution. Figs. 4 **a)** and **c)** combines the three curves of Fig. 3, showing CR and resolution plotted against RMSE. The results are shown for RMSE measurements with high (i.e. 10dB) and low (i.e. -10dB) SNR values. We observe that for a given RMSE, SWiP will yield a larger CR improvement and better resolution than GCF. Or, the other way around, for a given CR improvement or resolution, SWiP yields a lower RMSE than GCF. This is a specific advantage of SWiP over GCF, which is valid where one seeks to improve CR or resolution while obtaining a low RMSE for the magnitudes of actual targets in the image, i.e. while accurately estimating echo magnitudes. Similar test should be performed for any other performance metrics of interest, to determine the relationship between GCF and SWiP, performance-wise. Although outside the scope of this paper, it is worth noting that in Fig. 3 **b)**, it is the parameters corresponding to DAS that yield the optimal RMSE, even though SWiP is derived from a MMSE criterion. This is, however, consistent with the results in [22], which found that this class of MMSE estimator implementations do not actually improve MSE unless the initial SNR is very low.

We also investigate the performance of the algorithms when the data are affected by phase aberrations, which is the original application of both the CF and GCF methods. We use the aberration profile from [23] with parameters corresponding to weak aberrations (a correlation length of 2.46 mm and delays scaled to 21 ns rms/90 ns peak). Fig. 3 shows the effects of adjusting the parameters (K_0 and α) on CR and RMSE. We observe once again, in Fig. 3 **a)**, that the CR of GCF decreases rapidly for increasing values of K_0, while that of SWiP is relatively constant until α reaches its lowest value.

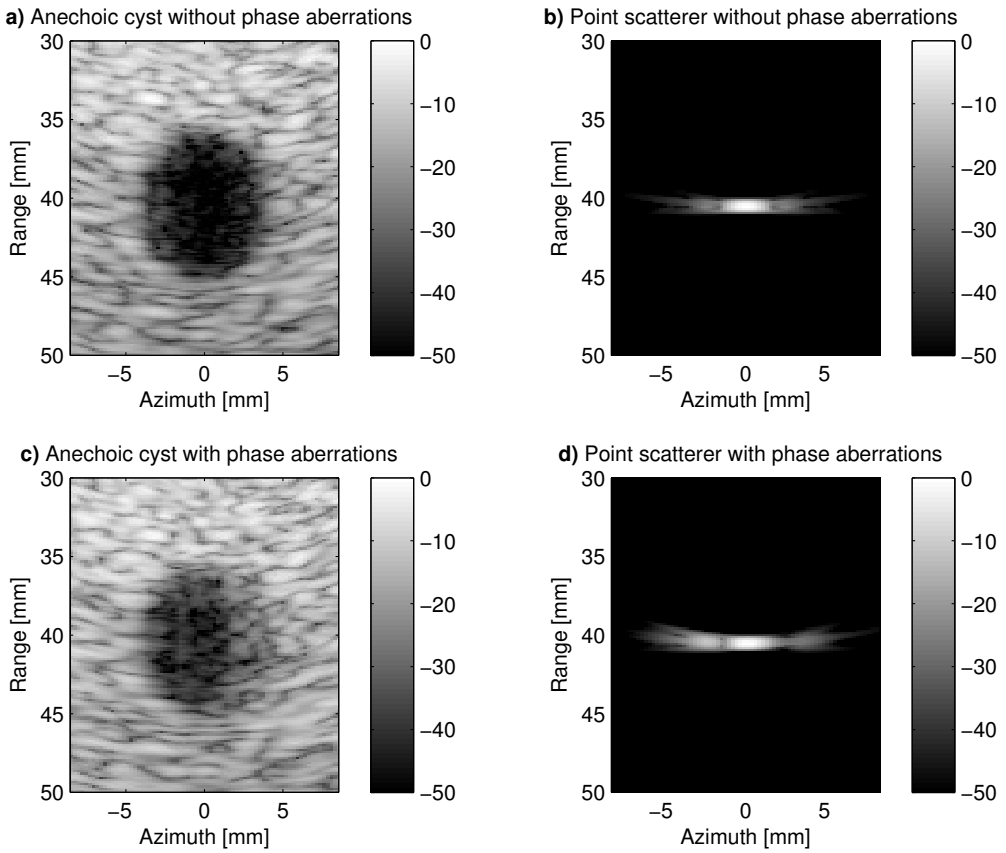

Fig. 2. **a)** DAS image of cyst without phase aberrations. **b)** DAS image of single point without phase aberrations. **c)** DAS image of cyst with phase aberrations. **d)** DAS image of single point with phase aberrations.

In Fig. 3 **c)** we see that the same is the case for resolution; the resolution of GCF converges rapidly to that of DAS, while SWiP experiences a slow convergence. The reduction of RMSE in Fig. 3 **b)** is more similar for the two methods. Fig. 4 **b)** and **d)** combines the different plots in Fig. 3, showing CR plotted against RMSE. We observe the same results as for no phase aberrations, i.e. SWiP generally yields superior CR and resolution for a given degree of robustness, or vice versa.

Note that we have not adressed the issue of choosing the optimal parameters α and K_0 for SWiP and GCF, respectively. This is an important issue that is outside the scope of this paper, but should be adressed in future research. Suffice it to say that our simulations show that performance is monotonically decreasing when adjusting the parameter to increase robustness, so any optimality criterion here should possibly be derived from the maximum allowable amount of image distortion, or some similar measure.

B. Computational Complexity

Because the different methods are based on different calculations, a brief comparison of computational complexity is required. The complexity of their origin, the coherence factor, is rather low. The numerator value of (4) is equal to the DAS output, which is already calculated as part of the beamformer output in (3). The denominator consists of M complex multiplications (squares) and $M-1$ real additions, and the final CF is calculated using 1 real division.

The denominator of the GCF has the same complexity as the denominator of the CF. However, the beams in the numerator must also be calculated. Depending on the number of non-broadside beams to be used, $2K_0$ this is most efficiently done using either an FFT or some appropriate form of direct calculation of the $2K_0$ desired beams.

The numerator and the first term in the denominator of the SWiP are equal to the DAS output, which we have argued that would be calculated either way. The remaining term, i.e. the second term of the denominator, consists of M complex subtractions, M complex squares, and $M-1$ real additions. This corresponds to an increase of M complex subtractions compared to CF. All in all, the differences between CF, GCF, and SWiP with respect to computational complexity are very small.

IV. Conclusions

We have compared two robust adaptions of the coherence factor; the generalized coherence factor and the scaled Wiener postfilter. Simulations show that when SWiP and GCF achieve identical robustness, SWiP will generally retain more of the

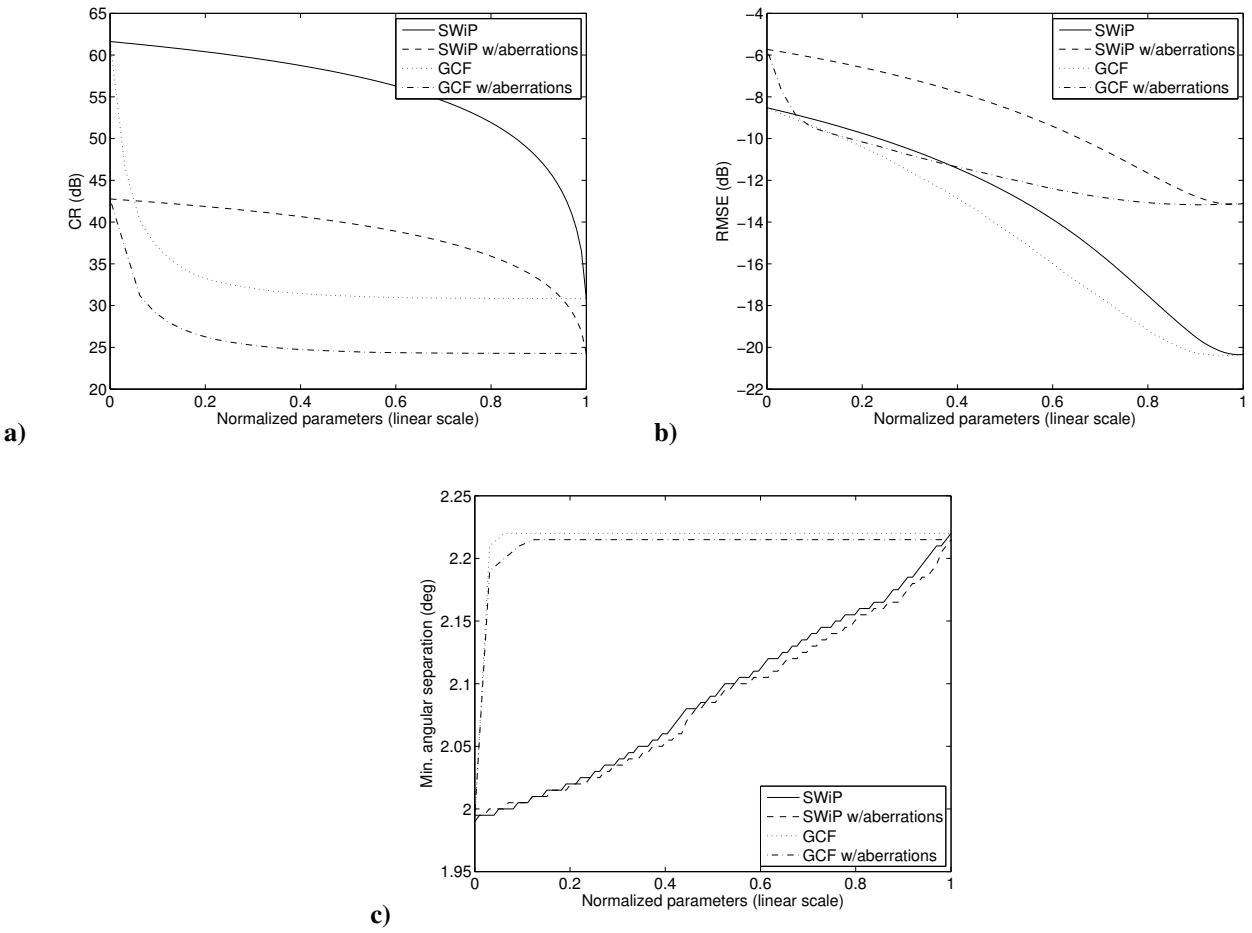

Fig. 3. Effects of parameter choice on CR, RMSE, and resolution for a ULA with $M = 64$ elements. **a)** CR. **b)** RMSE. **c)** Resolution. Shown for normalized parameters $\tilde{\alpha} = (M - \alpha)/M$ and $\tilde{K}_0 = 2K_0/M$.

desired performance of the CF than the GCF does, with respect to cyst contrast ratio and resolution improvements. Similar results were found both for the case of phase aberration reduction and for general noise reduction. Both CF, GCF, and SWiP were shown to have very similar computational complexity.

REFERENCES

[1] K. W. Hollman, K. W. Rigby, and M. O'Donnell, "Coherence factor of speckle from a multi-row probe," *Proc. IEEE Ultrasonics Symposium, pp. 1257-1260*, 1999.

[2] R. Mallart and M. Fink, "Adaptive focusing in scattering media through sound-speed inhomogeneities: the van cittert zernike approach and focusing criterion," *Journal of the Acoustical Society of America, Vol. 96, No. 6, pp. 3721-3732*, 1994.

[3] S. D. Silverstein, "Ultrasound scattering model: 2-d cross-correlation and focusing criteria - theory, simulations, and experiments," *IEEE Transactions on Ultrasonics, Ferroelectrics, and Frequency Control, Vo. 48, No. 4, pp. 1023-1030*, 2001.

[4] P.-C. Li and M.-L. Li, "Adaptive imaging using the generalized coherence factor," *IEEE Transactions on Ultrasonics, Ferroelectrics, and Frequency Control, Vol. 50, No. 2, pp. 128-141*, 2003.

[5] S.-L. Wang, C.-H. Chang, H.-C. Yang, Y.-H. Chou, and P.-C. Li, "Performance evaluation of coherence-based adaptive imaging using clinical breast data," *Ultrasonics, Ferroelectrics and Frequency Control, IEEE Transactions on*, vol. 54, no. 8, pp. 1669 –1679, august 2007.

[6] J. Camacho, M. Parrilla, and C. Fritsch, "Phase coherence imaging of grained materials," *Ultrasonics, Ferroelectrics and Frequency Control, IEEE Transactions on*, vol. 58, no. 5, pp. 1006–1015, May 2011.

[7] M. Klemm, J. Leendertz, D. Gibbins, I. Craddock, A. Preece, and R. Benjamin, "Microwave radar-based breast cancer detection: Imaging in inhomogeneous breast phantoms," *Antennas and Wireless Propagation Letters, IEEE*, vol. 8, pp. 1349 –1352, 2009.

[8] R. Burkholder and K. Browne, "Coherence factor enhancement of through-wall radar images," *Antennas and Wireless Propagation Letters, IEEE*, vol. 9, pp. 842 –845, 2010.

[9] S.-L. Wang and P.-C. Li, "MVDR-based coherence weighting for high-frame-rate adaptive imaging," *IEEE Transactions on Ultrasonics, Ferroelectrics, and Frequency Control, Vol. 56, No. 10, pp. 2097-2110*, 2009.

[10] B. M. Asl and A. Mahloojifar, "Minimum variance beamforming combined with adaptive coherence weighting applied to medical ultrasound imaging," *IEEE Transactions on Ultrasonics, Ferroelectrics, and Frequency Control, Vol. 56, No. 9, pp. 1923-1931*, 2009.

[11] S. Park, A. B. Karpiouk, and S. R. Aglyamov, "Adaptive beamforming for photoacoustic imaging using linear array transducer," *Proc. IEEE Ultrasonics Symposium, pp. 1088-1091*, 2008.

[12] J.-F. Synnevaag, A. Austeng, and S. Holm, "Adaptive beamforming applied to medical ultrasound imaging," *IEEE Transactions on Ultrasonics, Ferroelectrics, and Frequency Control, Vol. 54, No. 8, pp. 1606-1613*, 2007.

[13] C.-I. C. Nilsen and S. Holm, "Wiener beamforming and the coherence factor in ultrasound imaging," *Ultrasonics, Ferroelectrics and Frequency Control, IEEE Transactions on*, vol. 57, no. 6, pp. 1329 –1346, june 2010.

[14] J. Camacho, M. Parrilla, and C. Fritsch, "Phase coherence imaging," *Ultrasonics, Ferroelectrics and Frequency Control, IEEE Transactions on*, vol. 56, no. 5, pp. 958 –974, may 2009.

[15] M. Lediju, G. Trahey, B. Byram, and J. Dahl, "Short-lag spatial coherence of backscattered echoes: imaging characteristics," *Ultrasonics,*

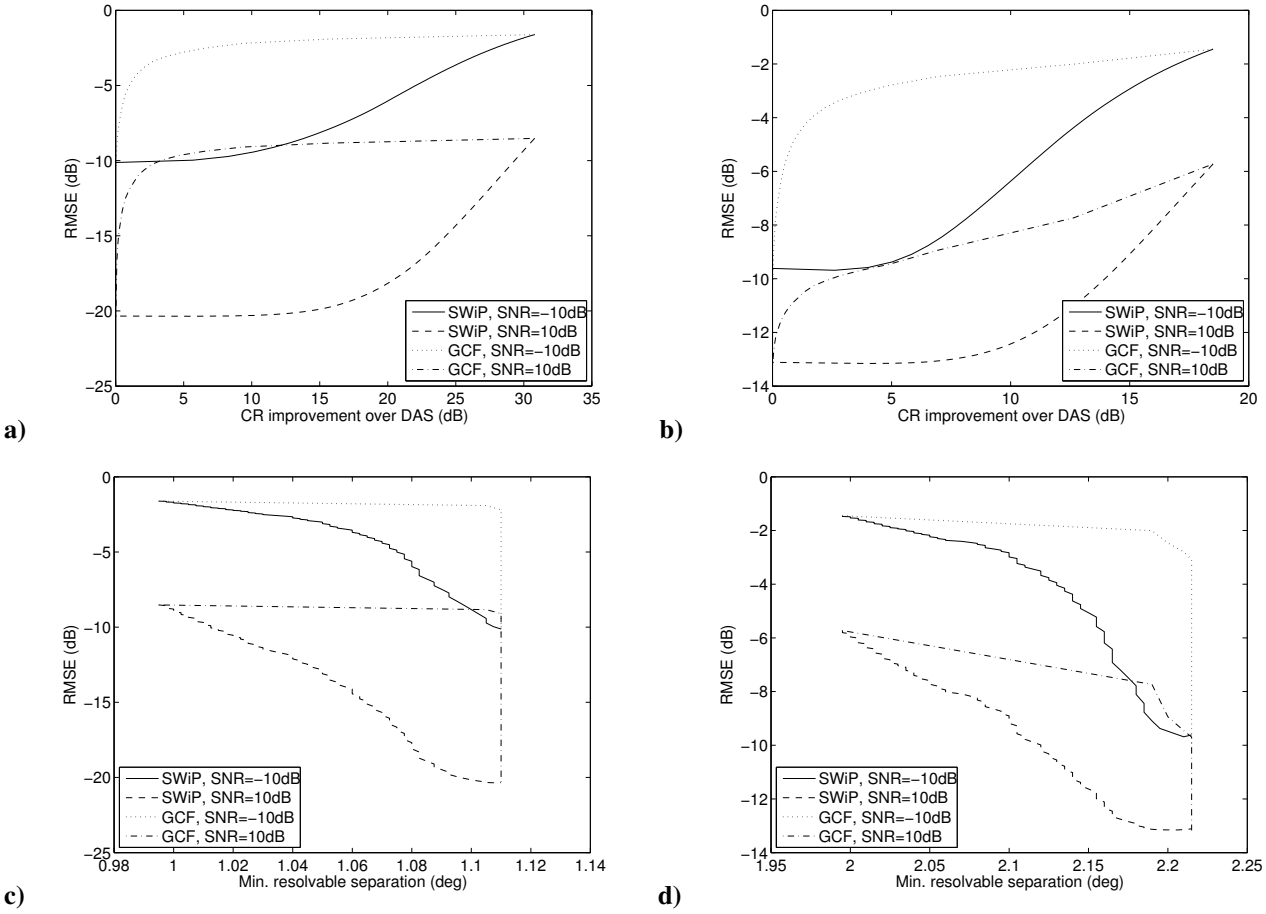

Fig. 4. Comparison of SWiP and GCF for $M = 64$ element ULA. **a):** RMSE vs. CR, without phase aberrations. **b)** RMSE vs. CR, with phase aberrations. **c):** RMSE vs. resolution, without phase aberrations. **d)** RMSE vs. resolution, with phase aberrations.

Ferroelectrics and Frequency Control, IEEE Transactions on, vol. 58, no. 7, pp. 1377 –1388, july 2011.

[16] J.-F. Synnevaag, A. Austeng, and S. Holm, "Benefits of high-resolution beamforming in medical ultrasound imaging," *IEEE Transactions on Ultrasonics, Ferroelectrics,and Frequency Control, Vol. 56, No. 9, pp. 1868-1879*, 2009.

[17] F. Vignon and M. R. Burcher, "Capon beamforming in medical ultrasound imaging with focused beams," *IEEE Transactions on Ultrasonics, Ferroelectrics, and Frequency Control, Vol. 55, No. 3, pp. 619-628*, 2008.

[18] C.-I. C. Nilsen and I. Hafizovic, "Beamspace adaptive beamforming for ultrasound imaging," *IEEE Transactions on Ultrasonics, Ferroelectrics, and Frequency Control, Vol. 56, No. 10, pp. 2187-2197*, 2009.

[19] M. O'Donnell and S. Flax, "Phase-aberration correction using signals from point reflectors and diffuse scatterers: measurements," *Ultrasonics, Ferroelectrics and Frequency Control, IEEE Transactions on*, vol. 35, no. 6, pp. 768 –774, nov 1988.

[20] J. Jensen, "Field: A program for simulating ultrasound systems," *Paper presented at the 10th Nordic-Baltic Conference on Biomedical Imaging Published in Medical & Biological Engineering & Computing, pp. 351-353, Volume 34, Supplement 1, Part 1*, 1996.

[21] J. Jensen and N. B. Svendsen, "Calculation of pressure fields from arbitrarily shaped, apodized, and excited ultrasound transducers," *IEEE Transactions on Ultrasonics, Ferroelectrics, Frequency Control, Vol. 39, pp. 262–267*, 1992.

[22] J. Thompson, "Some shrinkage techniques for estimating the mean," *Journal of the American Statistical Association*, pp. 113–122, 1968.

[23] A. Austeng, T. Bjastad, J.-F. Synnevaag, S.-E. Masoy, H. Torp, and S. Holm, "Sensitivity of minimum variance beamforming to tissue aberrations," *Proc. IEEE Ultrasonics Symposium, pp. 1072-1075*, 2008.

Carl-Inge C. Nilsen received the M.Sc. degree in 2005 and the Ph.D. degree in 2010, both in computer science, from the University of Oslo. From 2010 he has been working at the at the Department on Informatics, University of Oslo, as a post doctoral research fellow. His research interests include signal and array processing for ultrasound imaging and other acoustical applications.

Andreas Austeng was born in Oslo, Norway, in 1970. He received the M.S. degree in physics in 1996 and the Ph.D. degree in computer science in 2001, both from the University of Oslo. From 2001 he has been working at the at the Department on Informatics, University of Oslo, first as a post doctoral research fellow, and currently as an Associate Professor. His research interests include signal processing for acoustical imaging.